A stochastic study of microsolvation. I. Structures of CO in small argon clusters

F. Paesani, F. A. Gianturco, M. Lewerenz, and J. P. Toennies

Citation: The Journal of Chemical Physics **111**, 6897 (1999); doi: 10.1063/1.479983
View online: https://doi.org/10.1063/1.479983
View Table of Contents: http://aip.scitation.org/toc/jcp/111/15
Published by the American Institute of Physics

A stochastic study of microsolvation. I. Structures of CO in small argon clusters

F. Paesani
Department of Chemistry, The University of Rome, Città Universitaria, 00185 Rome, Italy

F. A. Gianturco[a)]
Department of Chemistry, The University of Rome, Città Universitaria, 00185 Rome, Italy

M. Lewerenz
Zentralinstitut fuer Angewandte Mathematik Forschungszentrum, Juelich GmbH, D-52425 Juelich, Germany

J. P. Toennies
Max-Planck-Institut für Strömungsforschung, Bunsenstrasse 10, D-37073 Göttingen, Germany

(Received 7 June 1999; accepted 6 July 1999)

Diffusion Monte Carlo (DMC) calculations of the intermolecular vibrational ground states of $CO(Ar)_n$ clusters with $n=1-12$, for CO $v=0$ are reported. The intermolecular degrees of freedom of the clusters are treated in full dimensionality and a pairwise additive potential surface is used in which the Ar–CO interaction is described by a recently developed scheme which combines density functional theory (DFT) with the long-range dispersion contributions obtained from the perturbative theory. The calculations yield intermolecular ground state energies, Ar density distributions, radial and angular density probability distributions. Optimal structures by Simplex minimization have been calculated to estimate zero point energy (ZPE) and quantum effects. © *1999 American Institute of Physics.* [S0021-9606(99)00337-2]

I. INTRODUCTION

The past decade has brought tremendous advance in the study of weakly bound states of atoms and molecules. One of the driving forces behind this research has been the need to understand how the properties of atomic or molecular clusters vary as a function of size, particularly the stepwise development of condensed phase attributes, thus allowing us to bridge the gap between isolated molecules and condensed matter. The experimental and theoretical methods which are now being applied to these systems are often capable of revealing quantum-state-specific information and are therefore quite different from those applied in the bulk, resulting in the promise that these finite systems will provide us with fundamentally new insight into condensed-phase behavior.

Originally dominated by theoretical studies on pure helium and hydrogen clusters,[1–5] the field has profited greatly from a number of recent scattering[6–8] and spectroscopic studies of clusters with embedded probe molecules.[9–12] These spectroscopic experiments were invariably carried out on clusters with several hundred to several thousand atoms and only few spectroscopic studies are dedicated to small van der Waals complexes.[13,14] Recently there has been considerable theoretical interest in the structure and energetics of rare-gas (Rg) clusters with embedded molecules (M).[3,15–17] The reason for this is that these clusters $[M(Rg)_n]$ possess a number of features which make them attractive to theoreticians. In fact, the relatively few degrees of freedom of the clusters permit theoretical treatments at the level of rigor and detail that would be impossible for liquids or matrices and furthermore both solute (M)–solvent (Rg) and solvent (Rg)–solvent (Rg) interactions are rather weak, dominated by pairwise additive two-body forces. Although the exact magnitude of nonpairwise additive, three-body forces is still an unresolved issue of great importance, those features greatly simplify the construction of intermolecular potentials.

As is well known, when two or more atoms or molecules coalesce to form a cluster, the associated bound states depend in a very sensitive way on the nature of the intermolecular forces between them. The bound state solutions are represented by eigenfunctions that have well-defined, time-independent energies. As a result, one often considers the bound state properties of molecules to be ''static,'' which is sometimes misinterpreted to mean the molecule is ''rigid.'' As recently also shown by us,[18] the bound states of a van der Waals complex are instead anything but rigid, often exhibiting large-amplitude motions.

While the triatomic bound state problem for a single potential energy surface (PES) is essentially solved (scarcity of reliable global PESs being the only, albeit serious, remaining problem), the situation is much less satisfactory for larger floppy clusters. The only methods available thus far for an accurate treatment of the quantum systems with very many degrees of freedom are based on stochastic approaches and are collectively referred to as quantum Monte Carlo,[19] Their main advantages are the absence of size-dependent properties and the favorable scaling of the computational effort with the number of degrees of freedom.

a)Author to whom correspondence should be addressed. Electronic mail: FAGIANT@CASPUR.IT

The purpose of the present work is therefore to accurately characterize for the first time the vibrational ground states of various $CO(Ar)_n$ clusters, with n from 1 to 12, employing the diffusion Monte Carlo (DMC) method. In our treatment no approximation is made on the quantum dynamics of all internal degrees of freedom of these van der Waals (vdW) clusters. We determine what are essentially the numerically exact ground state energies of $CO(Ar)_n$, for potentials which are superpositions of CO–Ar and Ar–Ar interactions. In addition, the ground state wavefunctions of these clusters are analyzed in terms of probability distributions of the internal coordinates, all of which indicate higly delocalized motion of the surrounding Ar atoms.

In Sec. II we describe a recently developed treatment which combines density functional theory (DFT) with the long-range dispersion interaction obtained from perturbative theory for the calculation of the full PES of CO–Ar system. In Sec. III we briefly explain the computational method employed to provide an accurate solution of the many-body Schrödinger equation, while we discuss the results of calculations carried out on the title system in Sec. IV.

II. THE INTERACTION POTENTIAL

The use of density functionals for the treatment of either hydrogen bonded or van der Waals systems has been much less widespread than the study of thermochemical data or molecular equilibrium geometries.[20]

It therefore becomes interesting to explore the applicability of any DFT theory to the broad range of configurations sampled by the intermolecular interactions in order to extend the possible use of *ab initio* methods to increasingly more complicated multielectron partners. One knows, in fact, that the inclusion of the all-important electron correlation effects occurs rather directly within DFT methods while it happens only slowly within configuration interaction (CI) expansions, where necessary truncations can often jeopardize the whole reliability of the final results.

One can begin by writing down the familiar expression for the total energy:[21,22]

$$E_{\mathrm{tot}}=E[\rho]=\sum_i \epsilon_i-\frac{1}{2}\int\frac{\rho(\mathbf{r})\rho(\mathbf{r}')}{|\mathbf{r}-\mathbf{r}'|}d\mathbf{r}d\mathbf{r}'+E_{\mathrm{xc}}[\rho]-\int V_{\mathrm{xc}}\rho(\mathbf{r})d\mathbf{r}, \tag{1}$$

where

$$\sum_i^N \epsilon_i=T_s[\rho]+\int V_{\mathrm{eff}}(\mathbf{r})\rho(\mathbf{r})d\mathbf{r}, \tag{2}$$

and

$$V_{\mathrm{eff}}(\mathbf{r})=V(\mathbf{r})+\int\frac{\rho(\mathbf{r}')}{|\mathbf{r}-\mathbf{r}'|}d\mathbf{r}'+V_{\mathrm{xc}}(\mathbf{r}), \tag{3}$$

where $V(\mathbf{r})$ is the potential energy between nuclei and electrons and $V_{\mathrm{xc}}(\mathbf{r})$ is the exchange-correlation potential energy. The above result is exact provided we know the kinetic energy functional form in Eq. (2) and the E_{xc} functional form in Eq. (1).[21] It is toward the solution of this specific aspect that many computational and theoretical efforts have been directed in recent years.[20,23] Here T_s is the sum of single-particle kinetic energy operators and E_{xc} is the nonclassical exchange and correlation energy contributions coming from the chosen form of the functional of the total electronic density $\rho(\mathbf{r})$ in the ground electronic state of the system.

The many possible forms that the E_{xc} contribution may take have been discussed at length by the relevant DFT literature[21,24–29] and will not be repeated here. It suffices to say that one can conventionally write it as:

$$E_{\mathrm{xc}}\simeq\tfrac{1}{2}E_x+\tfrac{1}{2}E_{\mathrm{xc}}^{\mathrm{LSDA}}, \tag{4}$$

where the $E_{\mathrm{xc}}^{\mathrm{LSDA}}$ contribution could be obtained from the formula proposed by Slater for the exchange part[27] and from a formula described by Vosko, Wilk, and Nusair[28] for the correlation, while the E_x contribution is the pure exchange energy of the Kohn–Sham (KS) orbitals from a single determinant.[29] This DFT evaluation of the interaction energy will be called Half–Half (HH) in the present discussion.[29]

The full calculation of the anisotropic interaction was therefore carried out by fixing, at first, the r_{CO} distance at 2.1323 a_0 (equilibrium bond distance) and by evaluating different orientations between $\theta=0°$ and $\theta=180°$. To introduce the vibrational dependence of CO, the same type of calculation has been repeated for the other six values of r_{CO} in order to include the first five diatomic vibrational states. In all the calculations of the present work the $\theta=0°$ orientation corresponds to the collinear Ar–C–O structure.

The quality of the Gaussian basis set expansion employed was of the quadruple-zeta (cc-pVQZ) level,[30] where the original and contracted sets of functions were, respectively: $(16s,11p,3d,2f,1g)$ and $[6s,5p,3d,2f,1g]$ on the Ar atom, $(12s,6p,3d,2f,1g)$ and $[5s,4p,3d,2f,1g]$ on the C atom, and $(12s,6p,3d,2f,1g)$ and $[5s,4p,3d,2f,1g]$ on the oxygen atom.

One important aspect of the full evaluation of the weak, vdW type of PES involves the inclusion of long-range (LR) dispersion contributions:

$$V_{\mathrm{DISP}}(r,R,\theta)=-\frac{C_6(r,\theta)}{R^6}-\frac{C_7(r,\theta)}{R^7}-\frac{C_8(r,\theta)}{R^8}, \tag{5}$$

where the coefficients, and their θ-dependence, have been often discussed in the literature.[31] As is well-known, this expression is valid only in the long-range limit. Thus, in order to have a full description of the dispersion contributions over a broader range of distances, we need to introduce first a general damping function[32] that modifies Eq. (5) as follows

$$V_{\mathrm{DISP}}(r,R,\theta)=-\sum_{n=6}^{8}\left[1-\sum_{k=0}^{n}\frac{(bR)^k}{k!}\exp(-bR)\right]\frac{C_n(r,\theta)}{R^n}, \tag{6}$$

where b is a distance scaling factor, taken to be the same as the parameter B in a Born–Mayer type repulsion potential,[33] on the ground that both the repulsion and the dispersion

TABLE I. Computed and estimated geometries for the minimum energy structure of the Ar–CO complex (see reference for details).

	D_e/cm^{-1}	R_{min}/Å	θ/deg
EGM+empirical corrections[a]	108.7(PP1) 140.7(PP2)	3.77 3.57	78 95
Atom–atom empirical rules[b]	110	3.63	103
(6-12) empirical potential+molecular mechanics[c]	158	3.81	131
Ab initio coupled pair calculations with 133 GTOS[d]	71	3.86	88
Ab initio MP4 with 98 GTOS plus bond functions[e]	109	3.70	80
Ab initio MP2 with 67 GTOS[f]	69	4.00	100
Ab initio MP4 with 137 GTOS[g]	96.3	3.74	98
Present calcs. (HHDSD)	89.6	3.82	81

[a]Reference 31.
[b]Reference 36.
[c]Reference 37.
[d]Reference 38.
[e]Reference 39.
[f]Reference 40.
[g]Reference 41.

damping are consequences of wavefunction overlap. In the following we assume the dependence on r_{CO} of each dispersion coefficient as described in Ref. 31.

There are many ways in which the LR dispersion tail can be smoothly joined onto the short range DFT interaction. However, because of the difference in anisotropy of the two types of interactions, the resulting PES will be mostly affected in the well region. Since the present potential is expanded into Legendre polynomials

$$V(r,R,\theta)=\sum_{\lambda} V_{\lambda}(r,R)P_{\lambda}(\cos\theta), \tag{7}$$

one could assume that the DFT short range region already contains, for each of the coefficients, the correct Coulomb, exchange, and correlation energy contributions as given within the prescription of Eq. (4). Hence, one can subtract the first two contributions from the Half–Half (HH) calculations for each of the multipolar coefficients of Eq. (6)[31] by carrying out additional separate Hartree–Fock (HF) calculations with the same basis set discussed before which had been employed to obtain the KS orbitals in the self-consistent-field (SCF) part of the full HH interaction. One can therefore write:

$$V_{\lambda}^{DFT}(r,R)=V_{\lambda}^{HH}(r,R)\simeq V_{\lambda}^{HF}(r,R)+V_{\lambda}^{corr}(r,R), \tag{8}$$

from which

$$V_{\lambda}^{HH}(r,R)-V_{\lambda}^{HF}(r,R)\simeq V_{\lambda}^{corr}(r,R). \tag{9}$$

If one further presumes that at least the behavior of the correlation forces is given realistically by the DFT calculations, then one could modify the perturbative dispersion terms of Eq. (6) by using the values from Eq. (9) to scale the latter terms in the long range region[21] while remembering that, as is known, no dispersion contributions are included in a DFT model. Hence the long range (LR) contributions could be rewritten using Eqs. (6) and (9)

$$V_{\lambda}^{LR}(r,R)=V_{\lambda}^{DISP}(r,R)+D_{\lambda}V_{\lambda}^{corr}(r,R). \tag{10}$$

Each final multipolar coefficient can therefore be obtained by matching the two regions at the points where, for each Legendre component, the logaritmic derivatives of the dispersion and correlation branches are equal, a requirement that produces the D_{λ} scaling factors which correct the V_{λ}^{DISP} radial dependence and make the potential continuous in that region, in analogy to what was attempted earlier by Parker and Pack[31]

$$V_{\lambda}(r,R)=\begin{cases} V_{\lambda}^{DFT}(r,R) & \text{for } R<R_{\lambda} \\ V_{\lambda}^{HF}(r,R)+V_{\lambda}^{LR}(r,R) & \text{for } R>R_{\lambda} \end{cases}. \tag{11}$$

Having defined in the above way the dispersion contributions, we obtained a modified DFT surfaces of the Ar–CO system which we shall call the Half–Half with damped scaled dispersion (HHDSD). The results from such calculations have been already discussed in detail considering the equilibrium bond distance for the CO molecule ($r=2.1323\,a_0$) either for the He–CO (Ref. 34) or Ar–CO (Ref. 35) systems. We clearly showed there that the present modified DFT potential model followed closely the best available potential functions for those systems.

We summarize in Table I the results for the global minimum geometry of the rigid-rotor energy surfaces already discussed in Ref. 35 where we see that there is still considerable uncertainty about the best value for such global minimum, although some qualitative consensus is beginning to get established on the existence of a *T*-shaped geometry and on the value of the coordinate R_{min} for the well position (between 3.74 and 4.0 Å).

III. THE STOCHASTIC MODEL

The diffusion Monte Carlo (DMC) method[42] has been extensively discussed in a number of articles.[19,43–45] We therefore refer the reader to that literature for a fuller discussion, while this section merely summarizes the main features of the method, our particular implementation, and some specific extensions developed for the present application.

The key idea of the DMC method is the isomorphism between the time-dependent many-body Schrödinger equation and a multidimensional reaction–diffusion equation with anisotropic diffusion coefficients. Introduction of imaginary time $\tau=it/\hbar$, shifting of the absolute energy scale by a quantity E_{ref}, and identification of the inverse mass terms with diffusion coefficients D_j and of the shifted potential $V(\mathbf{r})-E_{ref}$ with position-dependent rate terms $k(\mathbf{r})$ leads to the following equations which show this analogy:

$$i\hbar \frac{\partial \Psi(\mathbf{r},t)}{\partial t} = -\sum_j \frac{\hbar^2}{2m_j}\nabla_j^2 \Psi(\mathbf{r},t) + [V(\mathbf{r}) - E_{\mathrm{ref}}]\Psi(\mathbf{r},t), \tag{12}$$

$$\frac{\partial \Psi(\mathbf{r},\tau)}{\partial \tau} = -\sum_j \frac{\hbar^2}{2m_j}\nabla_j^2 \Psi(\mathbf{r},\tau) + [V(\mathbf{r}) - E_{\mathrm{ref}}]\Psi(\mathbf{r},\tau), \tag{13}$$

$$\frac{\partial C(\mathbf{r},t)}{\partial t} = -\sum_j D_j \nabla_j^2 C(\mathbf{r},t) + k(\mathbf{r})C(\mathbf{r},t). \tag{14}$$

Knowledge of the structure of the wavefunction can be fruitfully exploited for increased accuracy by introducing a guiding function Ψ_T approximating the true wavefunction. The introduction of Ψ_T results in additional drift terms in the diffusion equation which direct the random walkers into regions where the trial wavefunction is large. At the same time, the rate terms are now controlled by the local energy defined as

$$E_{\mathrm{local}}(\mathbf{r}) = \Psi_T^{-1}(\mathbf{r})\hat{H}\Psi_T(\mathbf{r}) = \Psi_T^{-1}(\mathbf{r})\hat{T}\Psi_T(\mathbf{r}) + V(\mathbf{r}), \tag{15}$$

which is a smoother function of the coordinates than the potential and reduces the variance of the energy estimators

$$\frac{\partial(\Psi\Psi_T)}{\partial \tau} = \left[\sum_j \frac{1}{2m_j}\nabla_j^2(\Psi\Psi_T) - \frac{1}{m_j}\nabla_j(\Psi\Psi_T \nabla \ln \Psi_T)\right] - [\Psi_T^{-1} T \Psi_T + V(\mathbf{r}) - E_{\mathrm{ref}}](\Psi\Psi_T). \tag{16}$$

This equation reduces to Eq. (13) for the trivial case $\Psi_T = 1$.

A random walk technique is used to calculate the steady-state solution of the diffusion equation corresponding to a given quantum problem. A large ensemble of random walkers is propagated with time steps $\Delta\tau$ starting from some arbitrary initial distribution. The propagation from τ to $\tau + \Delta\tau$ consists of random Gaussian displacements of the Cartesian coordinates and systematic moves under the influence of the quantum drift force $F(\mathbf{r}) = \Psi_T \nabla \ln \Psi_T$ and an update of a weight carried by each random walker. Additionally we use a Metropolis type acceptance check for each attempted move[44] such that for arbitrary time steps the number density of walkers is given by Ψ_T^2 in the limit of zero branching, while their weights are a stochastic sample of the local value of Ψ/Ψ_T. This has been shown to result in large reductions of the time step error of DMC calculations. Our implementation uses a global check after trial moves have been made for all particles. The short time approximation to the Green's function appropriate for Eq. (16) is

$$G(\mathbf{r}\rightarrow\mathbf{r}';\Delta\tau) = \prod_j \left[\left(\frac{m_j}{2\pi\Delta\tau}\right)^{3/2} \exp\left\{-\frac{m_j}{2\Delta\tau}\left(\mathbf{r}_j - \mathbf{r}'_j - \frac{\Delta\tau}{2m_j}\mathbf{F}_j(\mathbf{r})\right)^2\right\}\right] \times \exp\left\{-\Delta\tau_{\mathrm{eff}}\left(\frac{E_{\mathrm{local}}(\mathbf{r}) + E_{\mathrm{local}}(\mathbf{r}')}{2} - E_{\mathrm{ref}}\right)\right\}. \tag{17}$$

The modified time step $\Delta\tau_{\mathrm{eff}}$ appears in the growth term of Eq. (17) because not all moves attempted according to $G(\mathbf{r}\rightarrow\mathbf{r}';\Delta\tau)$ are accepted in the Metropolis step. Proposed moves from $\mathbf{r}$ to $\mathbf{r}'$ are carried out with probability

$$P(\mathbf{r}\rightarrow\mathbf{r}') = \min\{1, A(\mathbf{r}\rightarrow\mathbf{r}')\}, \tag{18}$$

$$A(\mathbf{r}\rightarrow\mathbf{r}') = \frac{|\Psi(\mathbf{r}')|^2 G(\mathbf{r}'\rightarrow\mathbf{r})}{|\Psi(\mathbf{r})|^2 G(\mathbf{r}\rightarrow\mathbf{r}')}. \tag{19}$$

The asymmetric transfer function $G(\mathbf{r}\rightarrow\mathbf{r}';\Delta\tau)$ has to be explicitly taken into account in this acceptance decision. The effective time step $\Delta\tau_{\mathrm{eff}}$ is defined through the ratio of accepted displacements and attempted displacements according to

$$\Delta\tau_{\mathrm{eff}} = \Delta\tau \frac{\langle \Delta\mathbf{r}^2\rangle_{\mathrm{acc}}}{\langle \Delta\mathbf{r}^2\rangle_{\mathrm{att}}}. \tag{20}$$

Our specific implemetation assigns a variable weight to each random walker. As a consequence of the exponential weight update the sum of weights $W(\tau) = \Sigma_i w_i(\tau)$ grows or decays according to the mismatch between E_{ref} and the average local energy.

Walkers whose relative weight $w_{\mathrm{rel}} = w_i / W(\tau)$ falls below a preselected value $w_{\min}$ are eliminated randomly from the ensemble with probability $p_- = 1 - w_{\mathrm{rel}}$ or retained and assigned the average weight $W(\tau)/n_{\mathrm{walk}}$ with probability $p_+ = w_{\mathrm{rel}}$. Walkers whose relative weight grows beyond a maximum value $w_{\max}$ are split into $n_w = \mathrm{int}(w_{\mathrm{rel}} + u)$ walkers of weight w_i / n_w, where u is a uniform random number. The values of $w_{\min}$ and $w_{\max}$ are chosen such that the average number of walkers remains approximately constant during the run, while the instantaneous ensemble fluctuates. These mechanisms ensure that the walkers remain concentrated in relevant regions of configuration space without introducing artificial sources or sinks and can be easily generalized to a situation with correlated walks on several surfaces.

After equilibration of the initial random walker distribution the ensemble average of E_{local} which will be referred as E_{mean} in this article is identical with the ground state energy irrespective of Ψ_T and is only subject to statistical fluctuations. The ground state energy can also be computed from the rate at which the total weight of the ensemble grows or decays as τ elapses. This estimator is called the growth energy

$$E_{\mathrm{growth}} = E_{\mathrm{ref}} - \frac{\partial \ln W(\tau)}{\partial \tau}, \tag{21}$$

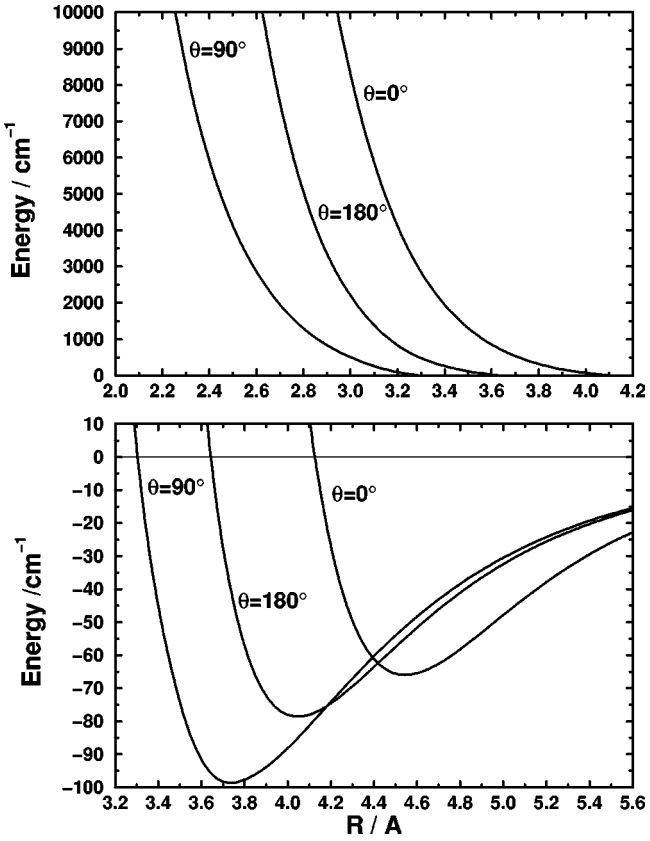

FIG. 1. Orientational behavior of the Ar–CO interaction employed in the present work. Upper panel: repulsive region at three different orientations. Lower panel: well regions for the same orientations. The $\theta=0°$ orientation corresponds to the linear Ar–C–O structure.

and is known to have a smaller time step dependence than E_{mean}. Both energy estimators were always extremely close to each other in our simulations, the difference never exceeding half the standard deviation of energies. We therefore report only our values for E_{mean} as E_0 values.

A. Calculation of expectation values

Arbitrary property expectation values $\langle\hat{A}\rangle$ are computed by replacing integrals by sums over samples

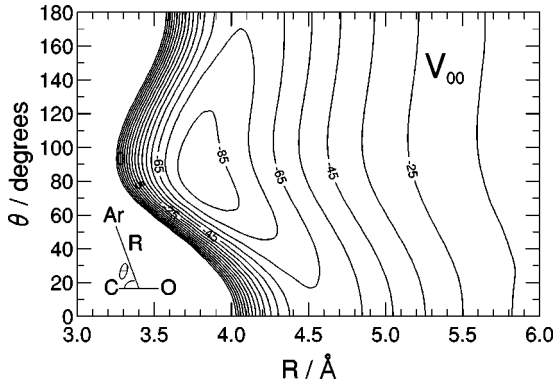

FIG. 2. Energy levels of the potential energy surface for the adiabatic V_{00} potential discussed in the main text. The energy levels are in units of cm^{-1}.

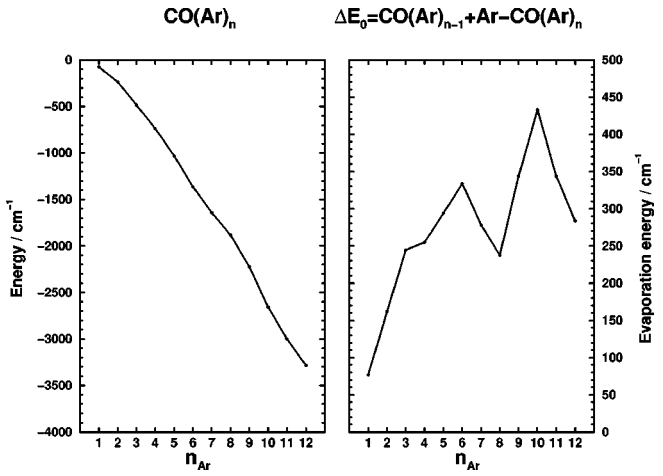

FIG. 3. Computed binding energies (left panel) and single-atom evaporation energies (right panel) from the DMC calculations, as a function of atom number in the $CO(Ar)_n$ clusters.

$$\langle\hat{A}\rangle=\frac{\int\Psi^*(\mathbf{r})\hat{A}\Psi(\mathbf{r})d\mathbf{r}}{\int|\Psi(\mathbf{r})|^2d\mathbf{r}}, \tag{22}$$

$$\approx\frac{1}{N}\sum_{i=1}^{N}\Psi^{-1}(\mathbf{r})\hat{A}\Psi(\mathbf{r}). \tag{23}$$

Only expectation values of local operators are directly accessible with the DMC scheme. In this case the integration reduces to an average over operator values $A(\mathbf{r})$

$$\langle\hat{A}\rangle\approx\frac{\Sigma_i^N w_i A(\mathbf{r}_i)}{\Sigma_i^N w_i}. \tag{24}$$

This technique is in particular applicable to the positional correlation functions which are very useful in visualizing the

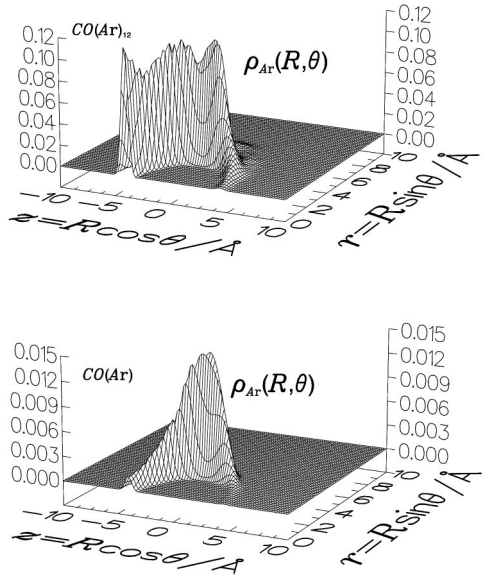

FIG. 4. 3D density distributions of Ar atoms around the CO molecule obtained from DMC calculations. Upper diagram: density values for $n=12$; lower panel: density values for the CO(Ar) cluster. Distances in Å.

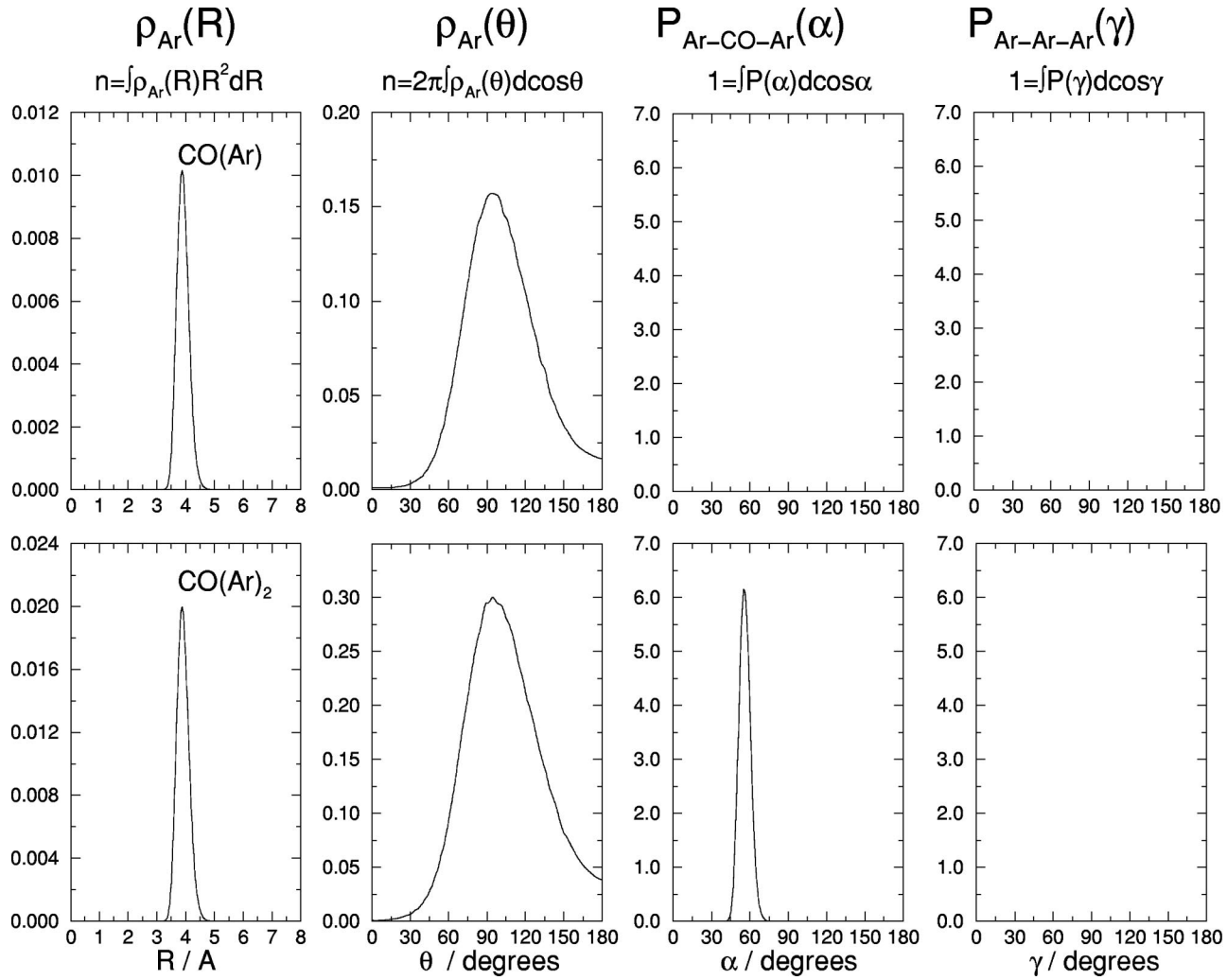

FIG. 5. Radial and angular density distributions for the $CO(Ar)_n$ clusters. Upper panels: for the $n=1$ case; lower panels: for the $n=2$ case. The panels represent, from left to right: radial distributions from the molecule center-of-mass; angular distributions for one Ar atom's Jacobi angle; angular distributions for two Ar atoms with respect to the molecular center-of-mass; angular distributions for three Ar atoms with respect to the middle atom of each trimer.

structure of the clusters. The radial distribution of rare-gas atoms relative to the center-of-mass of the whole cluster is computed as

$$P_{\mathrm{rad}}(R)=\frac{1}{n}\sum_{i}^{n}\left\langle \frac{\delta(R_i-R)}{R^2}\right\rangle_{\mathrm{walk}}. \tag{25}$$

The radial distribution function can be easily converted to the spherically averaged radial rare-gas density distribution $\rho(R)$

$$\rho(R)=\frac{n}{4\pi}P_{\mathrm{rad}}(R). \tag{26}$$

In a similar way we compute two-dimensional histograms in cylinder coordinates to analyze the density distribution $\rho(r,z)$ of argon atoms around the CO molecule. The CO bond is chosen at the z-axis and the perpendicular distance of argon atoms to this axis defines the polar radius r. The origin coincides with the center-of-mass (CM) of CO and the carbon atom is on the positive z-axis. The density distribution is computed as

$$\rho(r,z)=\frac{n}{2\pi}\sum_{i}\left\langle \frac{\delta(r_i-r)}{r}\delta(z_i-z)\right\rangle_{\mathrm{walk}}, \tag{27}$$

$$n=2\pi\int_{0}^{\infty}\int_{-\infty}^{\infty}\rho(r,z)r\,dr\,dz. \tag{28}$$

This quantity is accumulated on a grid which is equidistant in z and r^2 which eliminates the need to take square roots during the data collection.

B. The global potential energy function

All calculations were done with a purely pairwise additive potential energy surface based on the DFT *ab initio* part for the Ar–CO interaction and the empirical HFD-B potential for Ar.[46] For the Ar–CO interaction we used the adiabatic expression

$$V_{v=0}^{\mathrm{ArCO}}(R,\theta)=\langle V^{\mathrm{ArCO}}(R,\theta,r_{\mathrm{CO}})\rangle_{v=0}=V_{00}(R,\theta), \tag{29}$$

where the index $v=0$ indicates averaging over the CO ground state wavefunction obtained by solving the Schrö-

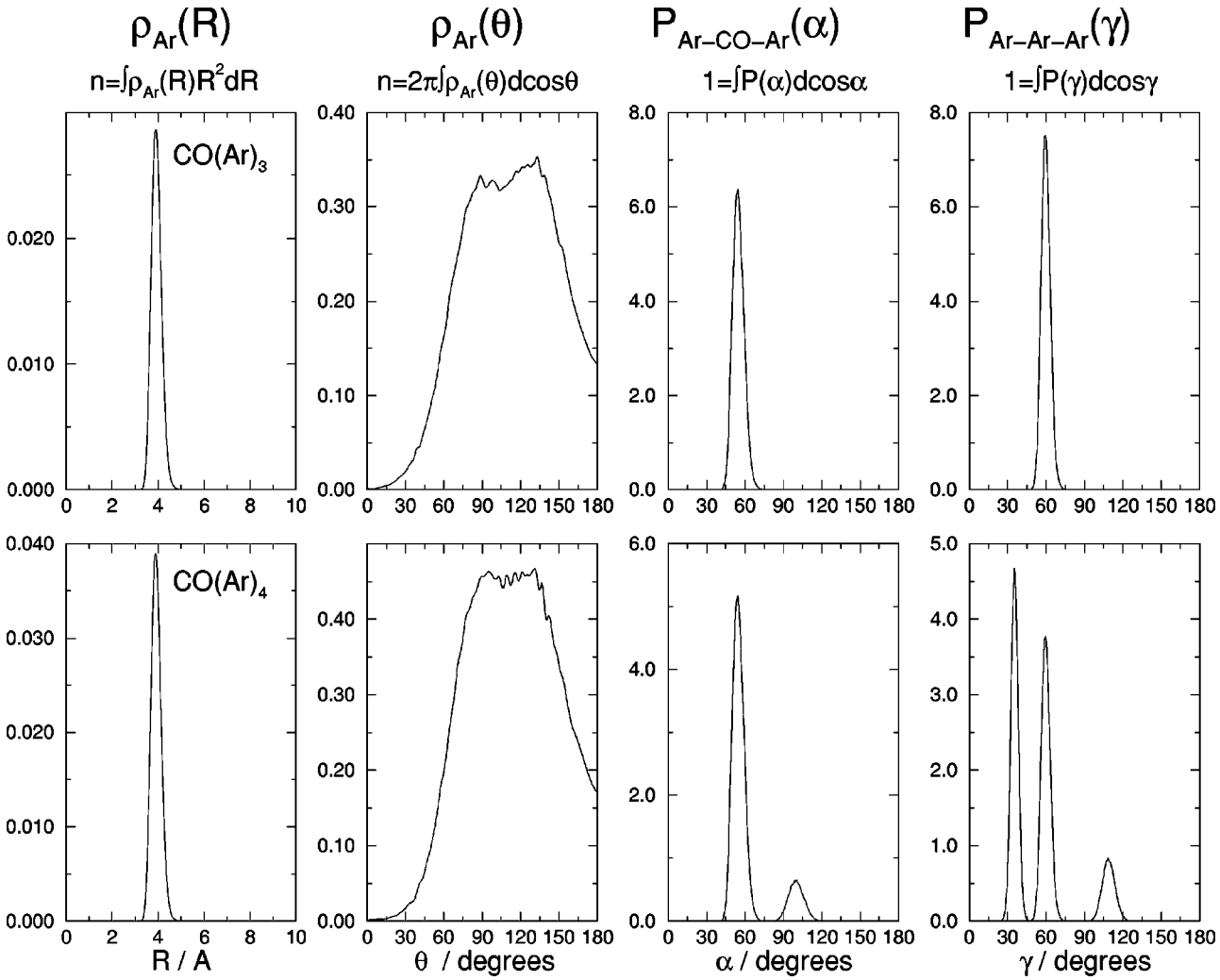

FIG. 6. Same as in Fig. 5 but for $n=3$ (upper panels) and $n=4$ (lower panels).

dinger equation for the diatomic potential of Ref. 47. Within this approximation the adiabatic potential of the $CO(Ar)_n$ cluster is now expressed as

$$V_{\text{total}}=\sum_{i=1}^{n} V_{v=0}^{\text{ArCO}}(R_i,\theta_i)+\sum_{i<j}^{n} V^{\text{ArAr}}(R_{ij}), \tag{30}$$

where R_{ij} are distances between rare-gas atoms i and j, and R_i, θ_i are Jacobi coordinates describing the distance between rare gas atom i and the center-of-mass of CO and the angle between the r_i vector and the CO bond vector. Although many-body forces are included in each term of the first sum on the r.h.s. of (30), no three-body or higher-order forces are added to it or to the second sum on the r.h.s. of Eq. (30). We shall further comment on this point when discussing the results from the present work.

In Fig. 1 we show the energy curves for three fixed orientations for the adiabatic potential V_{00}: in the lower panel we report the well region while the repulsive region is shown in the upper one. The adiabatic potential energy contours in (R,θ) is shown in Fig. 2 where one clearly sees that our calculations confirm the prevalence of a T-shaped configuration and the existence of a weak angular anisotropy as discussed in Ref. 41.

IV. DISCUSSION OF RESULTS

A. Binding and evaporation energies

Adiabatic ground state energies for $CO(Ar)_n$ when the CO molecule is in its vibrational state $v=0$, calculated from the DMC approach described in Sec. III, are shown in the left panel of Fig. 3 for clusters of different sizes. One clearly sees a change in the slope corresponding to $n=6$ and $n=10$. This fact becomes more evident when one looks at the single evaporation energy, that is the energy necessary to evaporate one Ar atom from the cluster. This quantity, that is a measure of the relative stability of clusters of different sizes, is shown in the right panel of the same figure. As mentioned before, it is possible to note there that the clusters with six and ten Ar atoms turn out to be relatively more stable than the others. It is also important to underline the relative instability for the $CO(Ar)_8$ cluster.

In Fig. 4 we report instead the 3D plot of the Ar density for the smallest $[CO(Ar)]$ and the largest $[CO(Ar)_{12}]$ cluster representing it in cylindrical coordinates. From these density distributions, the floppiness of such clusters is very clear which correspond to a diffuse distribution of the rare gas atoms around the CO molecule with a larger probability in

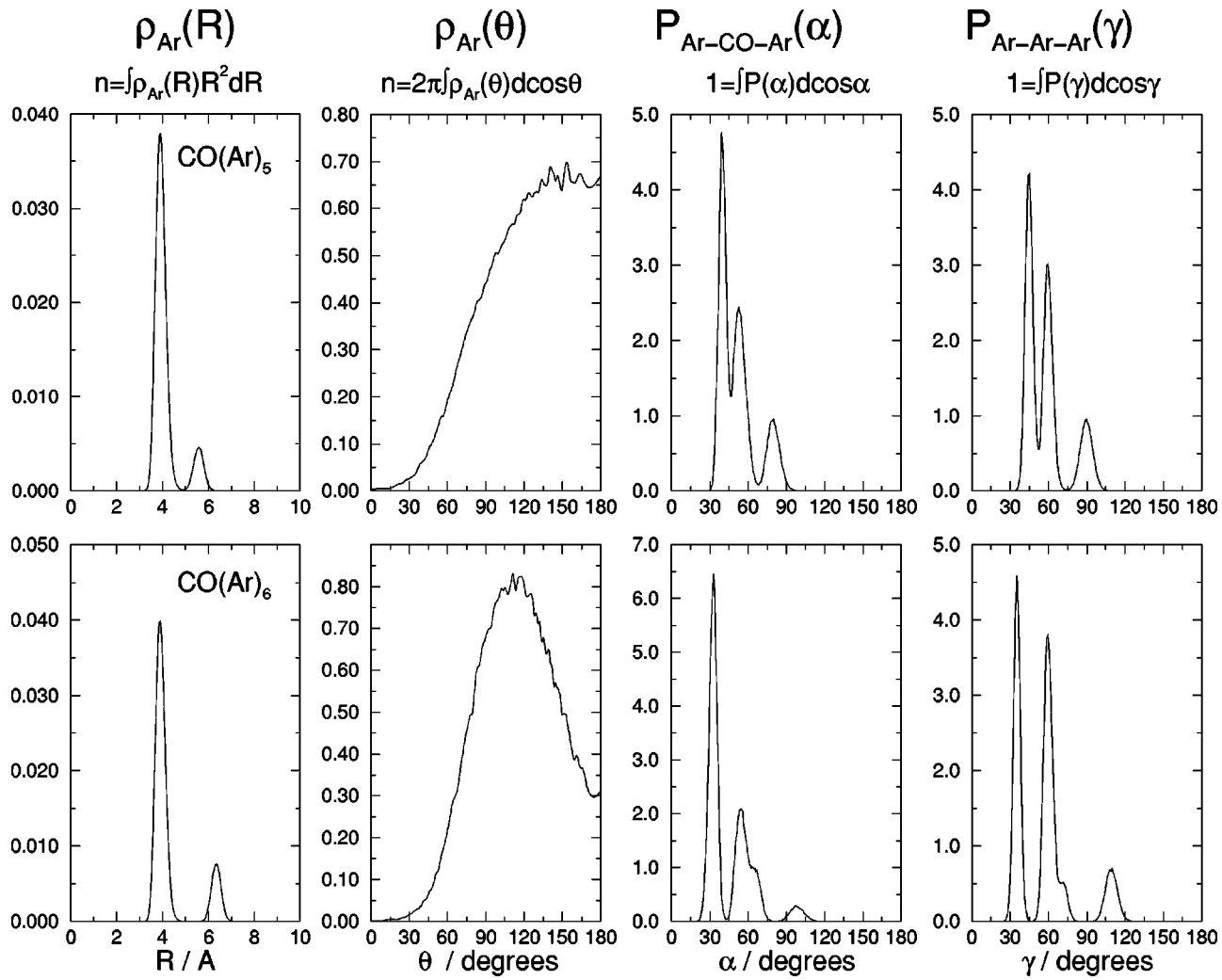

FIG. 7. Same as in Fig. 5 but for $n=5$ (upper panels) and $n=6$ (lower panels).

the region where the interaction is stronger. This is evident for the CO(Ar) cluster in which our calculations show a diffuse distribution of the Ar atom associated to all the orientations around the bond axis of the diatomic, that peak perpendicularly to this axis in the minimum region of the adiabatic potential surface. It is obviously more difficult to correspondingly locate for the $CO(Ar)_{12}$ cluster the mimimum of the multidimensional surface but is clear from the plot of the global density that the rare gas atoms are also distributed almost uniformly around the CO, providing a solvation shell for the diatomic impurity. This solvation can be further explained by looking at the strength of Ar–Ar and Ar–CO interactions. These interactions although very similar to each other, show in fact that the attractive part between Ar atoms is stronger than that for the Ar–CO portion and therefore the rare gas atoms in the clusters are distributed as shown by the calculations in order to optimize their own interactions.

B. Radial and angular correlation values

In order to obtain more information about the structure of the present clusters we have also analyzed the radial and the angular density distribution probability of the Ar atoms. In Figs. 5–10 we report in the first column the radial density distribution, in the second one the angular density distribution in which the θ angle corresponds to the angle between the axis bond and the vector which starts from the center-of-mass of CO. The third and fourth columns show instead the angular distribution probability in which the α angle is the angle between the center-of-mass of CO and two argon atoms and the γ angle is the angle between three Ar atoms.

Looking at the first column, one clearly sees that the largest peak of the radial density is centered at about 4.0 Å that corresponds to the region of the minimum for the Ar–CO interaction. It is also possible to note in some clusters the appearance of another smaller peak at larger distances: this can be explained in terms of the small difference that exists between the solvent–solvent and solvent–solute interactions and the preferential stabilization effects from the interactions between the argon atoms. This suggestion is confirmed when looking at the angular distributions: in the second column it is possible to see a diffuse distribution of rare gas atoms around the CO impurity, with an increasing probability to find Ar atoms at the oxygen side of diatomic (stronger attraction Ar–CO) as the cluster size is increased, while both the angular probability distributions of α and γ show several narrow peaks which increase in number when

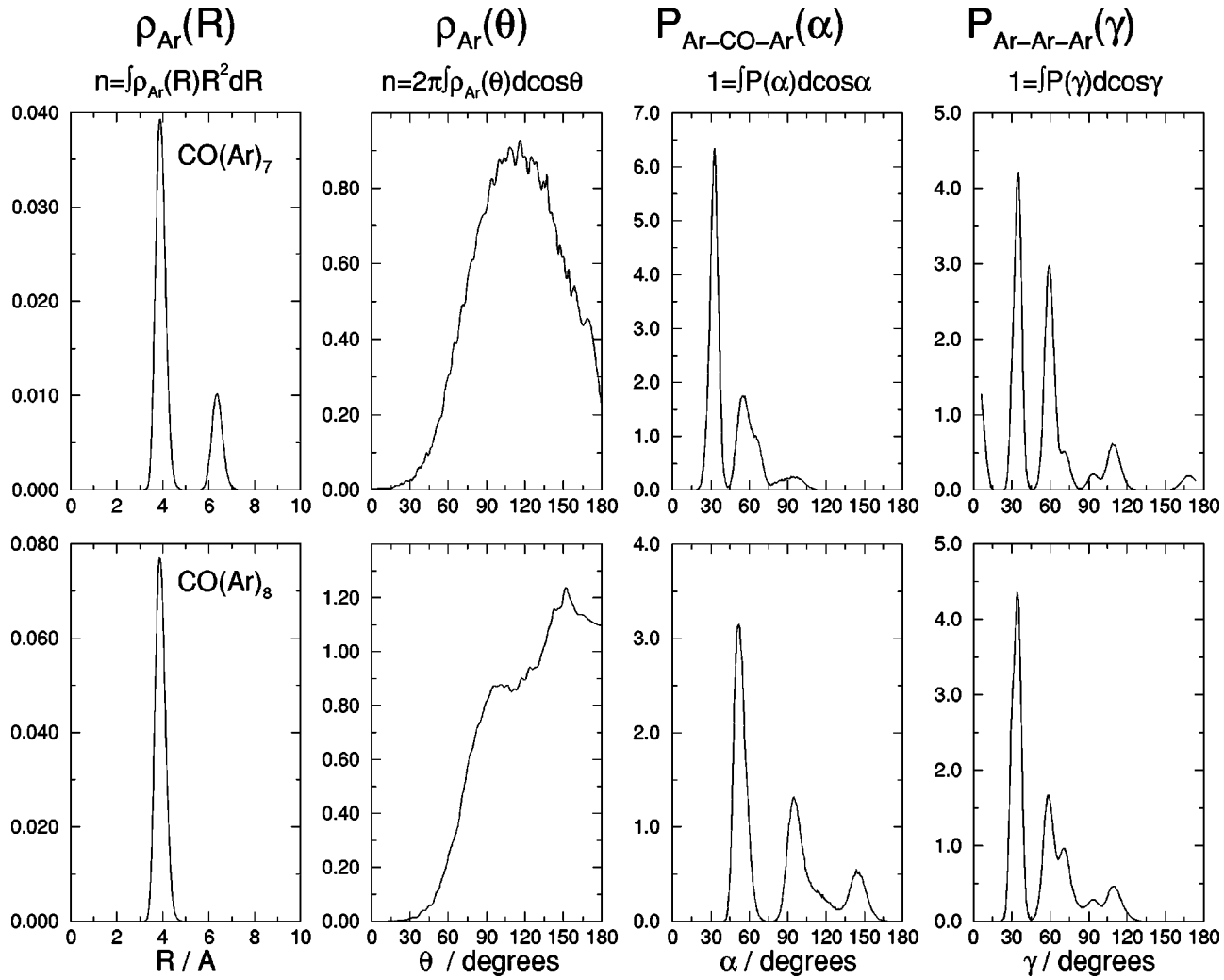

FIG. 8. Same as in Fig. 5 but for $n=7$ (upper panels) and $n=8$ (lower panels).

the size of cluster is increased. These results point at a pronounced solvation effect of Ar atoms on the CO as a ''solute'' and suggest besides that quantum effects are important in the vdW clusters where several minima exist and in which directional bonding cannot be described in terms of the usual ''balls and sticks'' picture for chemical bonding.

C. Optimal structures and quantum effects

In order to investigate further the quantum effects in the $CO(Ar)_n$ clusters we carried out numerically Simplex optimization[48] to find the ''classical'' optimal structures for such aggregates. In Figs. 11–12 we report the results of our calculations in terms of conventional bonding pictures with spheres describing the localized atoms. It is important to note at this point that we actually found several different structures for the same value of n which had total energies values below those of the ground state energy obtained from the DMC calculations, a rather common property for rare gas clusters.[49] It is possible to compare the Simplex structures, shown in Figs. 11 and 12, and the DMC results shown before. One clearly sees that for the smallest clusters it is still possible to find an analogy between classical and quantum geometries but when the number of Ar atoms increases the DMC results show very diffuse distributions of rare gas atoms that cannot be easily related to the structures obtained by the Simplex optimizations (see Figs. 11 and 12). This is further proof of the fact that the vdW clusters are not realistically described unless one takes in account the quantum effects. The presence of several, different cluster structures, for a given number of solvent atoms, that lie very close in energy and are separated by very small energy barriers, makes the classical picture of the clamped nuclei in the Born–Oppenheimer approximation very strongly dependent on the aggregate's temperature-annealing history. On the other hand, the quantum treatment using DMC calculations provides a physically more appealing description. This point can be demostrated by looking at Fig. 13 in which we report the zero point energy (ZPE) computed for the present clusters. One clearly sees that the ZPE plays an important role in their global energetics representing about 15%–20% of the total binding energy. One should also note that the Simplex minimization did not yield total energies that, for $n=11$ and 12, were below the DMC energies, a further sign of the presence of too many equivalent structures.

From the conventional structures of the Simplex con-

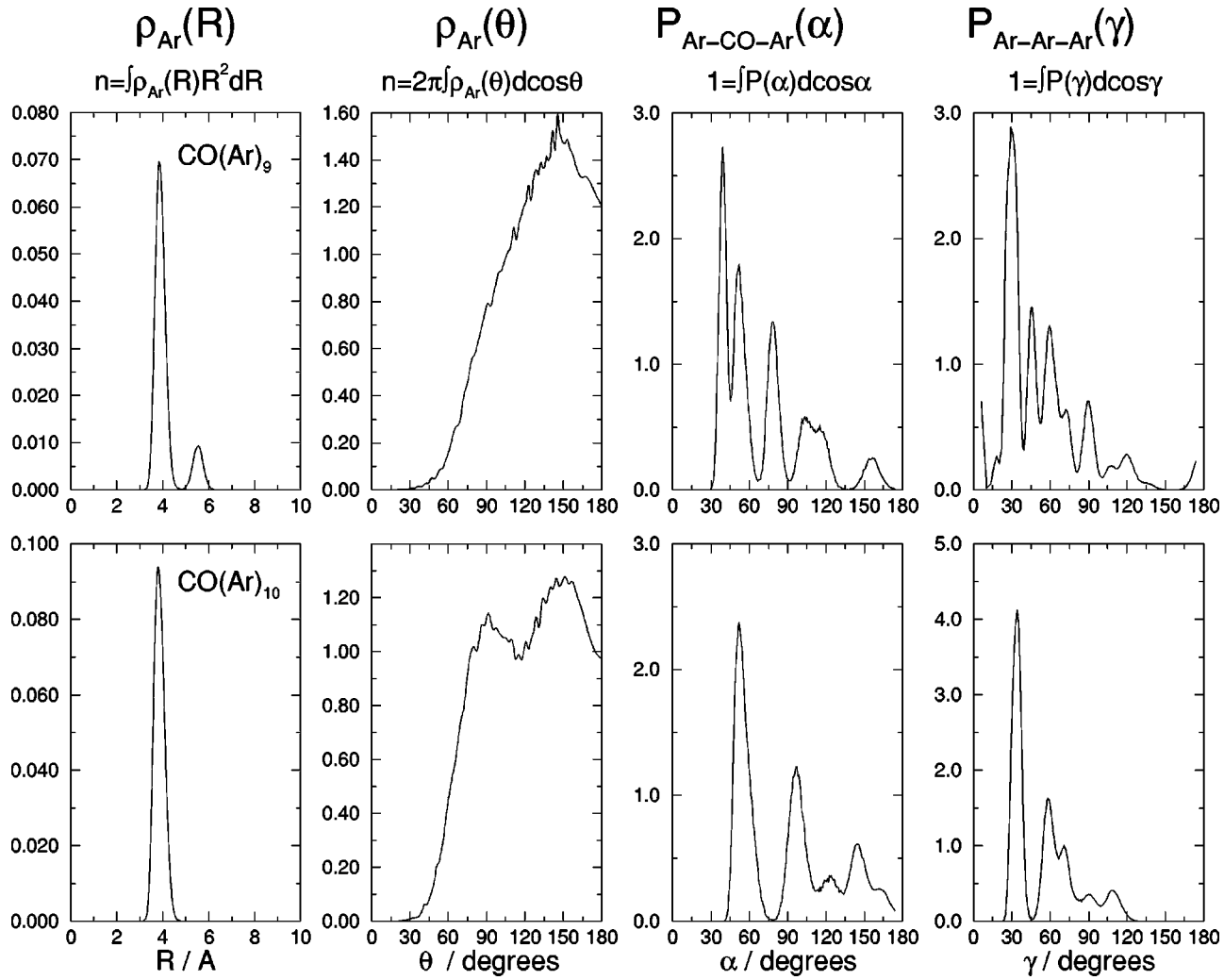

FIG. 9. Same as in Fig. 5 but for $n=9$ (upper panels) and $n=10$ (lower panels).

figurations, however, we can also draw some qualitative indicators on the behavior of the microsolvation process of CO molecules in argon as a ''solvent.'' We see, in fact, from Figs. 10 and 11 that the additional argon atoms which bind around the CO molecule, as the clusters grow bigger, tend to localize all on one side of the molecule since the stabilizing effect of the Ar–Ar attractive potential prevails over the competing Ar–CO stabilization. It therefore follows that, once the first two atoms are localized on a given side of the molecule the additional ones continue to enrich that side before the cluster gets to be big enough that repulsion effects among ''solvent'' atoms together with the increased contribution from solute–solvent attractive dispersion forces manage to locate additional atoms on the opposite side of the molecule, thereby ''solvating'' the CO in the Ar moiety.

Furthermore, we see that the Ar atoms initially prefer a *T*-geometry slightly shifted on the carbon side of CO and that the clusters grow by further adding the solvent atoms on that same side, thereby forming global clusters where the oxygen atom is, classically speaking, slightly pushed on the outer region of them. On the other hand, the quantum DMC results show angularly broad binding regions which are shifted on the oxygen side. Hence, the microsolvation of CO appears to start preferentially on the carbon atom, while the quantum picture tells us that the oxygen end of the molecule is instead the ''hydrophilic'' part of the CO as a solute.

V. CONCLUSIONS

Pairwise additive intermolecular PES for $CO(Ar)_n$ clusters, $n=1-12$, has been constructed from higly accurate Ar–Ar interaction[46] and anisotropic Ar–CO potential obtained by a recently developed treatment which combines density functional theory (DFT) with the long-range dispersion interaction.[35] As discussed in Ref. 35 this approach indicates that the use of DFT calculations combined with a global damping function yields a final PES (HHDSD) which is remarkably close to the best MC-SCF results[41] that are obtained with a greater computational effort.

Since the Ar–CO potential depends on the vibrational quantum number of CO we have followed the adiabatic treatment of Ref. 17 to investigate the energies and the structures for $CO(Ar)_n$ clusters in the CO vibrational state $v=0$ using the diffusion Monte Carlo (DMC) method. We have analyzed the relative stability of clusters of different size and the

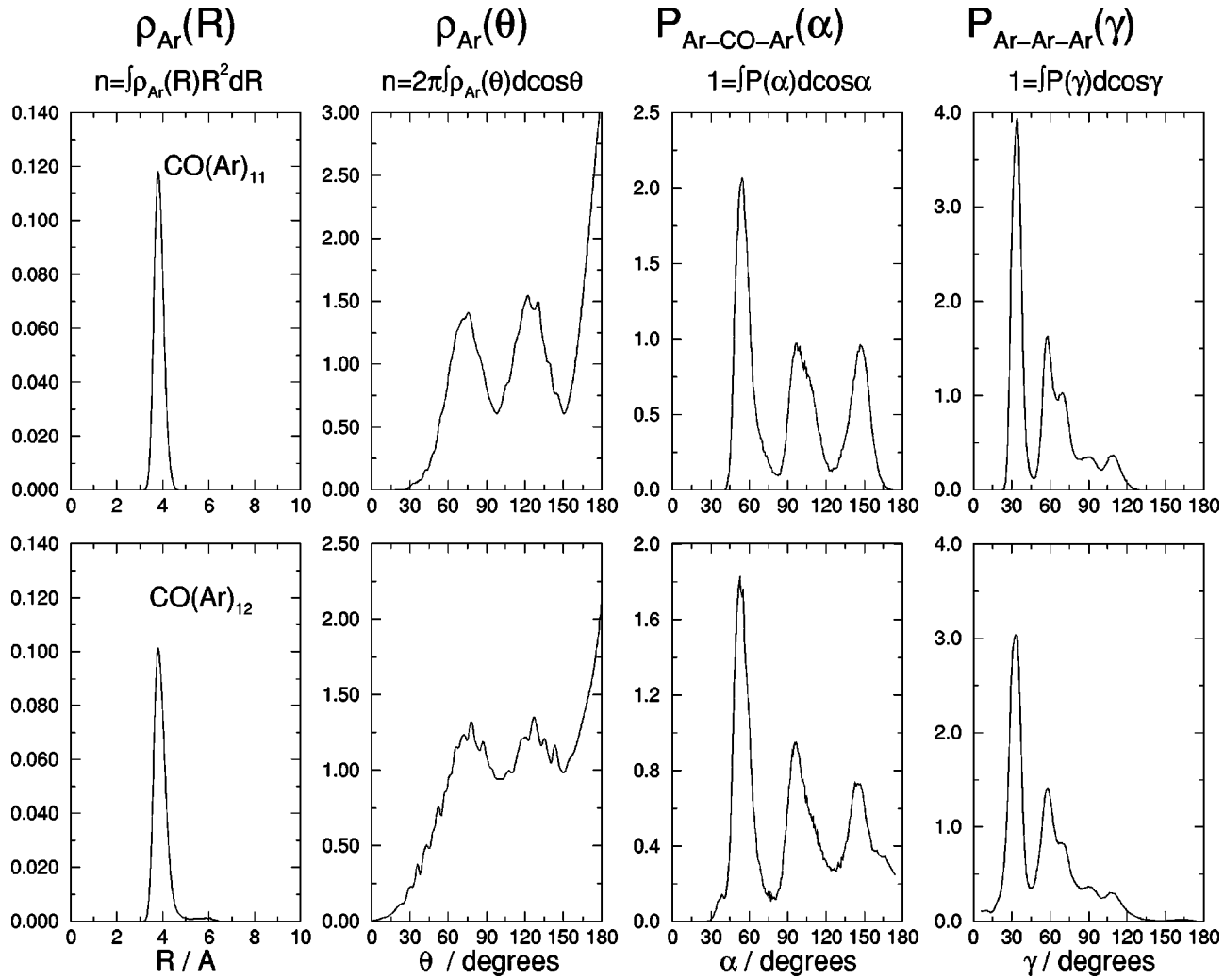

FIG. 10. Same as in Fig. 5 but for $n=11$ (upper panels) and $n=12$ (lower panels).

distributions of Ar atoms around the CO molecule. The comparison with the optimal structures obtained by Simplex minimization[48] is also reported.

We have then shown that, in such van der Waals clusters with several shallow minima separated by low isomerization barriers, the wave function associated with the ground bound state has significant amplitude at configurations which are spatially and energetically far from the equilibrium geometry. As a result, the global minimum of the full interaction no longer defines uniquely the structure of the complex and indeed the very notion of a molecular structure which would be described by the usual representation in terms of clamped

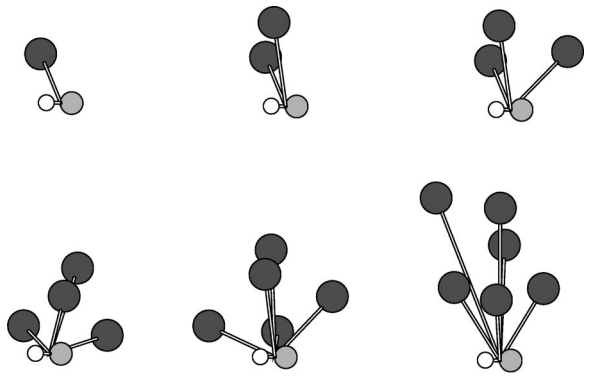

FIG. 11. Simplex optimization structures for the $CO(Ar)_n$ clusters using the interactions described in the main text. Top row, from left to right: the clusters with n from 1 to 3. Lower row, from left to right: the clusters with n from 4 to 6.

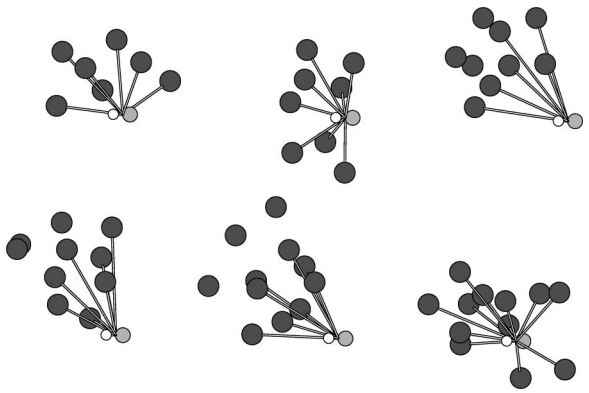

FIG. 12. Same as in Fig. 11 but for the Simplex structures of the clusters with $n=7$ to 9 (top row) and with the clusters with $n=10$ to 12 (bottom row).

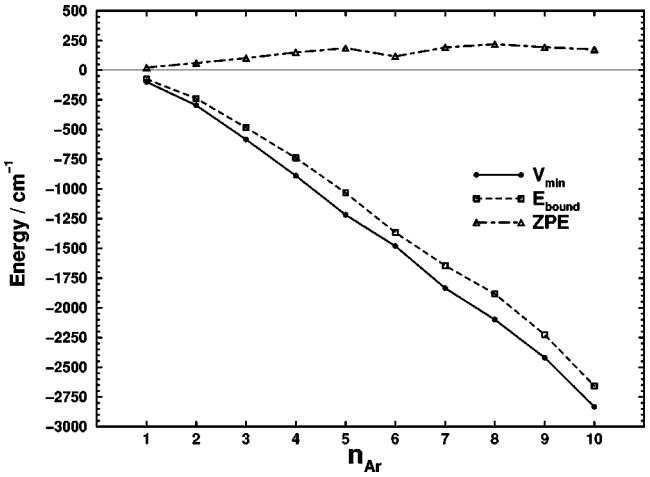

FIG. 13. Computed total energies as a function of cluster size (with n from 1 to 10). Solid line: from the Simplex minimum structures; dashed line: from the DMC calculations. Top panel: resulting zero-point energies from the calculations of the lower panel. All values in cm^{-1}.

nuclei and localized bonds, certainly a cornerstone of conventional chemistry, becomes ambiguous and has to be used with caution.

Another interesting aspect of the present work concerns the evaluation of the vibrational frequency shift caused by the cluster environment on the solute CO molecule. We have carried out specific calculations on this problem by employing the adiabatic approximation[17] but we will report them more extensively in a following publication.[50]

ACKNOWLEDGMENTS

The financial support of the Italian National Research Council (CNR), the Italian Ministry for University and Research (MURST), and the CASPUR Supercomputing Consortium is gratefully acknowledged. One of us (F.A.G.) thanks the Max-Planck-Gesellshaft for the award of the Max-Planck Research Prize (1995).

[1] V. R. Pandharipande, J. G. Zabolittzky, S. C. Pieper, R. B. Wiringa, and U. Helmbrecht, Phys. Rev. Lett. **50**, 1676 (1983); V. R. Pandharipande, S. C. Pieper, and R. B. Wiringa, Phys. Rev. B **34**, 4571 (1986).
[2] K. B. Whaley, Int. Rev. Phys. Chem. **13**, 41 (1994).
[3] S. A. Chin and E. Krotscheck, Phys. Rev. B **52**, 10405 (1995); E. Krotscheck and S. A. Chin, Chem. Phys. Lett. **227**, 143 (1994).
[4] D. M. Ceperley, Rev. Mod. Phys. **67**, 279 (1995).
[5] M. McMahon and K. B. Whaley, Chem. Phys. **182**, 119 (1994).
[6] A. Scheidemann, B. Shilling, and J. P. Toennies, J. Phys. Chem. **97**, 2128 (1993).
[7] M. Lewerenz, B. Schilling, and J. P. Toennies, Chem. Phys. Lett. **206**, 381 (1993).
[8] M. Lewerenz, B. Schilling, and J. P. Toennies, J. Chem. Phys. **102**, 8191 (1995).
[9] S. Goyal, D. L. Schutt, and G. Scoles, Phys. Rev. Lett. **69**, 933 (1992).
[10] F. Stienkemeier, J. Higgins, W. E. Ernst, and G. Scoles, Phys. Rev. Lett. **74**, 3592 (1995); J. Chem. Phys. **102**, 615 (1995).
[11] R. Fröchtenicth, J. P. Toennies, and A. Vilesov, Chem. Phys. Lett. **229**, 1 (1994); M. Hartmann, R. E. Miller, J. P. Toennies, and A. Vilesov, Phys. Rev. Lett. **75**, 1566 (1995).
[12] M. Hartmann, F. Mielke, J. P. Toennies, A. Vilesov, and G. Benedek, Phys. Rev. Lett. **76**, 4560 (1996).
[13] C. M. Lovejoy and D. J. Nesbitt, J. Chem. Phys. **93**, 5387 (1990).
[14] J. I. Cline, B. P. Reid, D. D. Evard, N. Sivakumar, N. Halberstadt, and K. C. Janda, J. Chem. Phys. **89**, 3535 (1988); W. D. Sands, C. R. Bieler, and K. C. Janda, *ibid.* **95**, 729 (1991); D. G. Jahn, S. G. Clement, and K. C. Janda, *ibid.* **101**, 283 (1994).
[15] R. N. Barnett and K. B. Whaley, J. Chem. Phys. **96**, 2953 (1992); M. A. NcMahon, R. N. Barnett, and K. B. Whaley, *ibid.* **104**, 5080 (1996); M. A. McMahon and K. B. Whaley, *ibid.* **103**, 2561 (1995); Y. Kwon, D. M. Ceperley, and K. B. Whaley, *ibid.* **104**, 2341 (1996).
[16] F. Dalfovo, Z. Phys. D **14**, 263 (1989).
[17] Z. Bačić, M. Kennedy-Mandziuk, J. W. Moskowitz, and K. E. Schmidt, J. Chem. Phys. **97**, 6472 (1992); P. Niyaz, Z. Bačić, J. W. Moskowitz, and K. E. Schmidt, Chem. Phys. Lett. **252**, 23 (1996); D. Blume, M. Lewerenz, F. Huisken and M. Kaloudis, J. Chem. Phys. **105**, 8666 (1996).
[18] F. A. Gianturco, M. Lewerenz, F. Paesani, and J. P. Toennies, Chem. Eur. J. **5**, 405 (1999).
[19] B. L. Hammond, W. A. Lester, Jr., and P. J. Reynolds, *Monte Carlo Methods in Ab Initio Quantum Chemistry* (World Scientific, Singapore, 1994).
[20] T. Ziegler, Chem. Rev. **91**, 651 (1991).
[21] R. G. Parr and W. Yang, *Density Functional Theory of Atoms and Molecules* (Oxford University Press, Oxford, 1989).
[22] S. Lundquist and N. H. March, *Theory of Inhomogeneous Electron Gas* (Plenum, New York, 1989).
[23] *Density Functional Methods in Chemistry*, edited by J. Labonowski and J. Andzelm (Springer, Heidelberg, 1991).
[24] J. Harris, Phys. Rev. A **29**, 1648 (1988).
[25] O. Gunnarsson and B. I. Lundquist, Phys. Rev. B **13**, 4274 (1976).
[26] A. D. Becke, J. Chem. Phys. **88**, 1053 (1976).
[27] J. C. Slater, *Self-Consistent Field of Molecules and Solids* (McGraw-Hill, New York, 1974).
[28] S. M. Vosko, L. Wilk, and M. Nusair, Can. J. Phys. **58**, 200 (1980).
[29] A. D. Becke, J. Chem. Phys. **98**, 1372 (1993).
[30] T. H. Dunning, Jr., J. Chem. Phys. **90**, 1007 (1989); D. E. Woon and T. H. Dunning, Jr., *ibid.* **98**, 1358 (1993).
[31] G. A. Parker and R. T Pack, J. Chem. Phys. **68**, 1585 (1978).
[32] K. T. Tang and J. P. Toennies, J. Chem. Phys. **80**, 3726 (1984).
[33] A. J. Stone, *Intermolecular Forces* (Clarendon, Oxford, 1996).
[34] F. A. Gianturco, F. Paesani, M. L. Laranjeira, M. A. Cunha, V. Vassilienko, A. G. Shashkov, and F. Zolotoukhina, Mol. Phys. **92**, 957 (1997); F. A. Gianturco, F. Paesani, M. L. Laranjeira, V. Vassilienko, M. A. Cunha, A. G. Shashkov, and F. Zolotoukhina, *ibid.* **94**, 605 (1998).
[35] F. A. Gianturco, F. Paesani, M. L. Laranjeira, M. A. Cunha, and V. Vassilienko, J. Chem. Phys. **110**, 7832 (1999).
[36] K. Mirsky, Chem. Phys. **46**, 45 (1980).
[37] C. A. Parish, J. D. Augspurger, and C. E. Dykstra, J. Phys. Chem. **96**, 2069 (1992).
[38] G. Jansen, Chem. Phys. Lett. **223**, 377 (1994).
[39] B. Kukawska-Tarnawska, G. Chalasinski, and K. Olszewski, J. Chem. Phys. **101**, 4964 (1994).
[40] V. Castells, N. Halberstadt, S. K. Shin, R. A. Beandet, and C. Wittig, J. Chem. Phys. **101**, 1006 (1994).
[41] S. Shin, S. K. Shin, and F.-M. Tao, J. Chem. Phys. **104**, 183 (1996).
[42] J. Anderson, J. Chem. Phys. **63**, 1499 (1975).
[43] D. M. Ceperley and B. Alder, Science **231**, 555 (1986); S. A. Chin, Phys. Rev. A **42**, 6991 (1990); M. A. Suhm and R. O. Watts, Phys. Rep. **204**, 293 (1991); W. A. Lester, Jr. and B. L. Hammond, Annu. Rev. Phys. Chem. **41**, 283 (1990).
[44] P. J. Reynolds, D. M. Ceperley, B. J. Alder, and W. A. Lester, Jr., J. Chem. Phys. **77**, 5593 (1982).
[45] C. J. Umrigar, M. P. Nightingale, and K. J. Runge, J. Chem. Phys. **99**, 2865 (1993).
[46] R. A. Aziz and M. J. Slaman, Mol. Phys. **58**, 679 (1986).
[47] P. Huxley and J. N. Murrell, J. Chem. Soc., Faraday Trans. 2 **79**, 323 (1983).
[48] W. H. Press, B. P. Flannery, S. A. Teukolsky, and W. T. Vetterling, *Numerical Recipes in Fortran*, 2nd ed. (Cambridge University Press, Cambridge, 1992).
[49] D. J. Wales and J. P. K. Doyl, J. Phys. Chem. **101**, 5111 (1997).
[50] F. Paesani and F. A. Gianturco (unpublished).